

The evolution of Drift Chambers at e^+e^- Colliders

(lessons learnt from a ≥ 40 -years long experience)

F. Grancagnolo
INFN – Lecce

INSTR20: Instrumentation for Colliding Beam Physics
Budker Institute of Nuclear Physics, Novosibirsk, Russia

24 - 28 February, 2020

INSTR2020

BINP, Novosibirsk

ВЕДА 1973-1968
ВЭП-1 1963-1968
CBX 1967-1967
ВЭП-2 1967-1967
ВЕДА 1992-2007
ВЭП-2000 2008
LHC 2008

Outline of the talk

➤ Performance evolution

- Momentum Resolution
- dE/dx , dN/dx and PId
- Mechanical Structure (X_0)
- FE and RO Electronics → NOT NOW

❖ Only Cylindrical Drift Chambers

- No **Planar** Drift Chambers
- No **Time Projection** Chambers
- No **Time Expansion** Chambers
- No **Radial** Drift Chambers:
radial wires – H1-forward/HERA
radial drift – ASTERIX/CERN
- No **Straw Tube** Cyl. Chambers (GlueX, PANDA)

❖ Only e^+e^- colliders

- No **fixed target** configurations (MEG2)
- No **ep and pp colliders** (AFS, CDF-CTC/COT)

❖ Layout Evolution

- From **single** sense wire cell, to **multiple** sense wires and **jet** cell configurations - and back to **single** sense wire cell
- **Axial-stereo** and **full stereo** layer configuration (KLOE, 4th-Concept, MEG2, IDEA)

❖ Gas mixture Evolution

- From **Argon** to **Helium** based gas

❖ Mechanical Structure and Wires Evolution

- ❖ **Read-out: from first clusters timing to Cluster Counting and Cluster Timing**

Trackers at e^+e^- Colliders

past

SPEAR	MARK2	Drift Chamber
	MARK3	Drift Chamber
DORIS	PLUTO	MWPC
	ARGUS	Drift Chamber
CESR	CLEO1,2,3	Drift Chamber
VEPP2/4M	CMD-2	Drift Chamber
	KEDR	Drift Chamber
	NSD	Drift Chamber
PETRA	CELLO	MWPC + Drift Ch.
	JADE	Drift Chamber
	PLUTO	MWPC
	MARK-J	TEC + Drift Ch.
	TASSO	MWPC + Drift Ch.
TRISTAN	AMY	Drift Chamber
	VENUS	Drift Chamber
	TOPAZ	TPC

PEP	MARK2	Drift Chamber
	PEP-4	TPC
	MAC	Drift Chamber
	HRS	Drift Chamber
	DELCO	MWPC
BEPC	BES1,2	Drift Chamber
LEP	ALEPH	TPC
	DELPHI	TPC
	L3	Si + TEC
OPAL	OPAL	Drift Chamber
	MARK2	Drift Chamber
SLC	SLD	Drift Chamber
	KLOE	Drift Chamber
DAPHNE	KLOE	Drift Chamber
PEP2	BaBar	Drift Chamber
KEKB	Belle	Drift Chamber

present

VEPP2000	CMD-3	Drift Chamber
VEPP4	KEDR	Drift Chamber
BEPC2	BES3	Drift Chamber
S.KEKB	Belle2	Drift Chamber

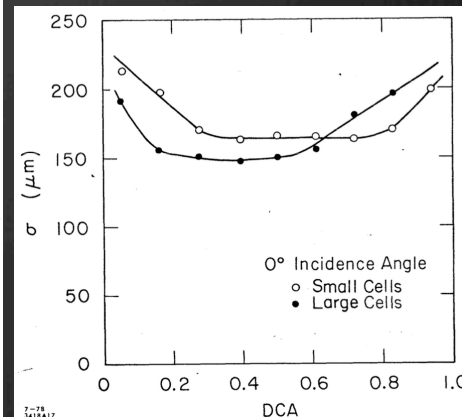
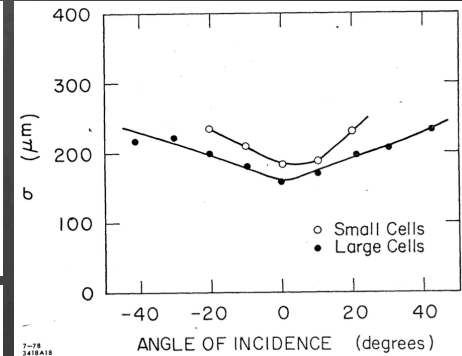
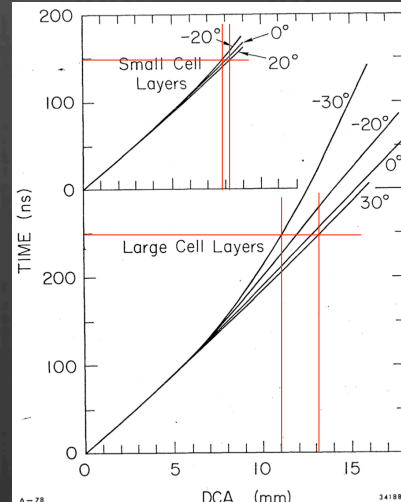
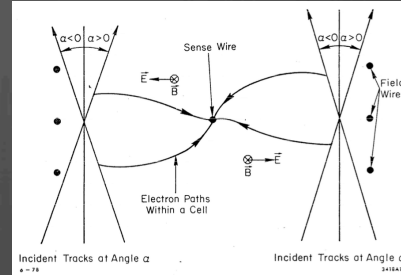
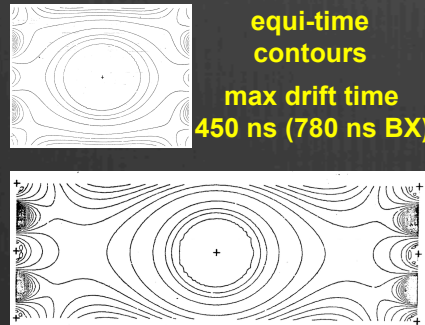
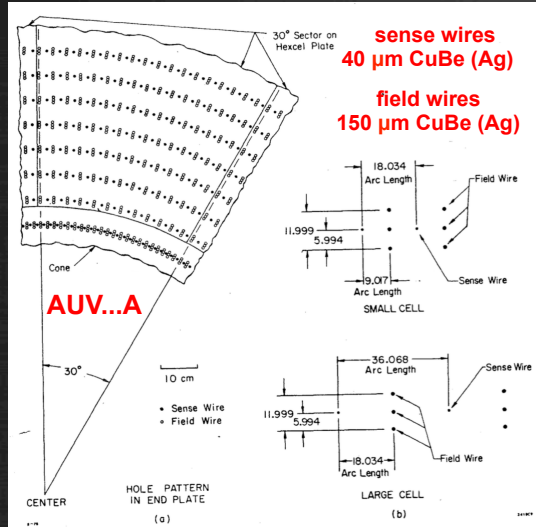
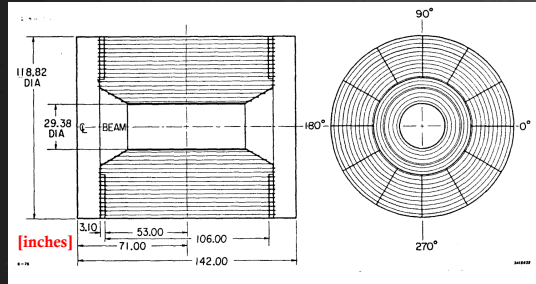
future

ILC	ILD	TPC
	SID	Si
CLIC	CLIC	Si
	CLD	Si
FCC-ee	IDEA	Drift Chamber
	Baseline	TPC
CEPC	IDEA	Drift Chamber
SCTF	BINP	Drift Chamber
STCF	HIEPA	Drift Chamber

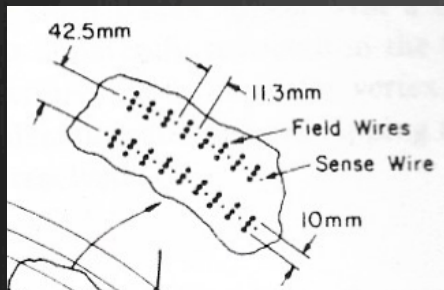
MARK II at SPEAR (1978) where it all began ...

A Large Cylindrical Drift Chamber for the Mark II Detector at SPEAR - Davies-White, W.A. *et al.* Nucl.Instrum.Meth. 160 (1979) 227

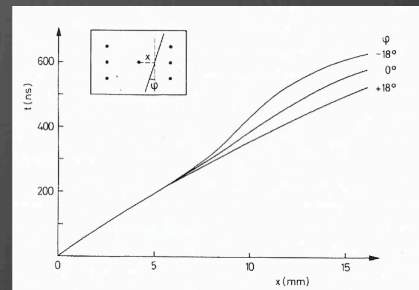
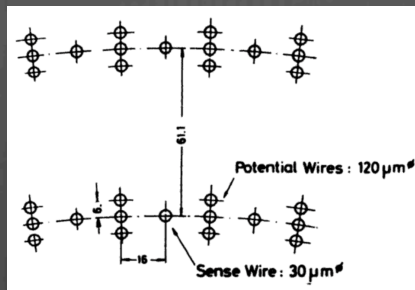
Single sense wire cell
 ≈ 3 m diameter
 ≈ 2.7 m active length
 0.41 Tesla B-field
 16 layers
 6 axial + 10 stereo (±3°)
 3204 drift cells (3:1)
 22,000 wires
 50% Ar – 50% C₂H₆
 2% X₀ radial - 20% X₀ e.p.



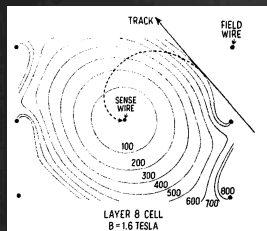
Single sense wire "open" cells 3:1



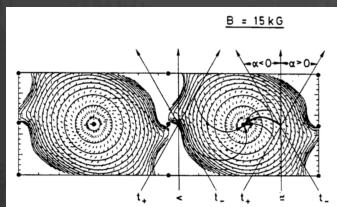
CLEO
CESR
1979



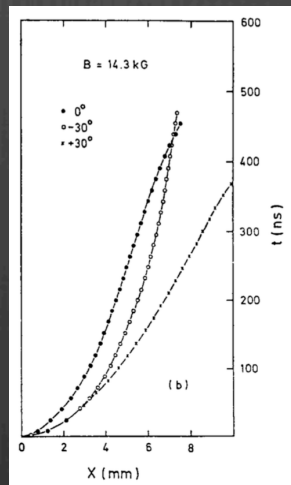
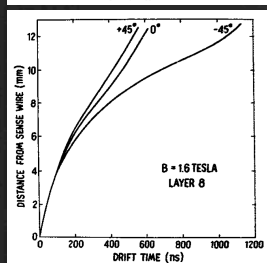
TASSO
PETRA
1979



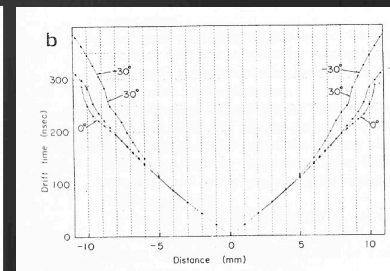
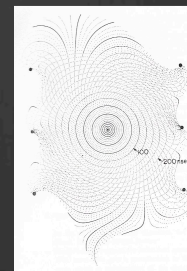
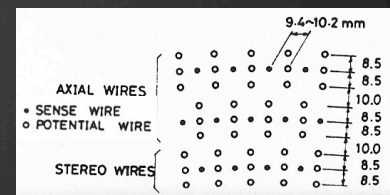
HRS
PEP
1980



CELLO
PETRA
1980



VENUS
TRISTAN
1983



Single sense wire "open" cells 3:1

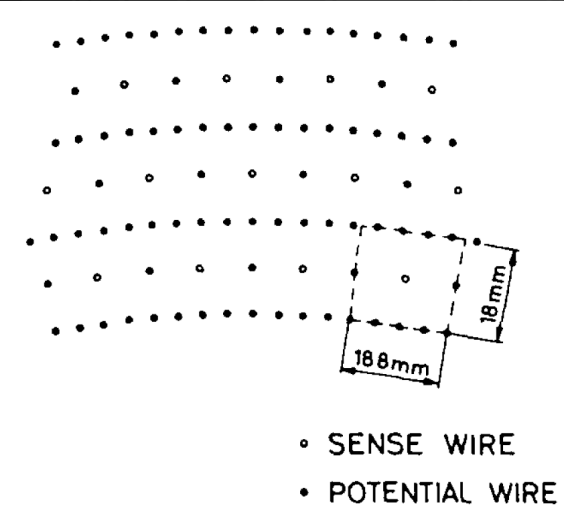
Mechanics

	MARK II SPEAR (1978)	CLEO CESR (1979)	TASSO PETRA (1980)	CELLO PETRA (1980)	HRS PEP (1980)	VENUS TRISTAN (1985)
Inner Radius [mm]	370	172	320	170	152	250
Outer Radius [mm]	1450	950	1280	700	1100	1260
Length [mm]	2700	1930	3450	2200	2540	3000
Axial layers	6	9	9	7	7	20
Stereo layers	10	8	6	0	8	9
Stereo angles [mrad]	±52	±52	±70	0	±60	±60
Number of sense wires	3204	5304	2340	1312	2448	7104
Total number of wires	13,000	22,000	9,000	5,200	10,000	28,000
sense wires [μm]	40 Cu-Be(Ag)	20 W(Au)	30 W(Au)	20 W(Au)	37 W(Au)	30 W-Re(Au)
field wires [μm]	150 Cu-Be(Ag)	115 Cu-Be(Ag)	120 Mo(Au)	50-100 Cu-Be	127 Cu-Be(Au)	125 Cu-Be(Au)
Inner cylinder [mm/X ₀]	3.2 Lexan / 0.9%		5 fiberglass/ 3%		1 Be / 0.3%	1 C-f / 0.5%
Outer cylinder [mm/X ₀]	6.25 Al / 7%		6.0 Al / 7%		0.6 Al / 0.7%	5 C-f / 2.4%
End-plates [mm/X ₀]	6.35 Al (cone) 3.2 Al + ... / 20%		35 Al / 39%		9.5 Al (cone) 15.9 Al / 18%	21 Al / 24%

Single sense wire "open" cells 3:1 Performance

	MARK II SPEAR (1978)	CLEO CESR (1979)	TASSO PETRA (1980)	CELLO PETRA (1980)	HRS PEP (1980)	VENUS TRISTAN (1985)
B-field [T]	0.4	1.0	0.5	1.3	1.6	0.75
Cell Size [mm²]	(9÷18)×12	11.3×10	16×12	15×18	17×10 ÷ 25×12	19×17
Gas Mixture	50 Ar / 50 C ₂ H ₆	50 Ar / 50 C ₂ H ₆	90 Ar / 10 CH ₄	90 Ar / 10 CH ₄	89 Ar / 10 CO ₂ / 1 CH ₄	50 Ar / 50 C ₂ H ₆
Spatial Resolution [μm]	150-200	250	220	170	200	150
Momentum Resolution	0.010p / 0.0145	0.012p / 0.007	0.020p / ?	0.029p / ?	0.005p / 0.003	0.0088p / 0.0012
Δp [MeV/c] at 1 GeV/c	17.6	13.9	>20.0	>30.0	5.8	14.9
dE/dx	//	6.5%	//	//	TOF + Cer.	//

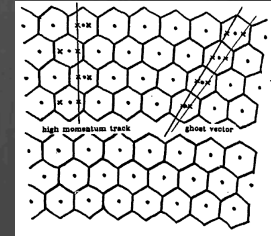
From "open" to "closed" cells



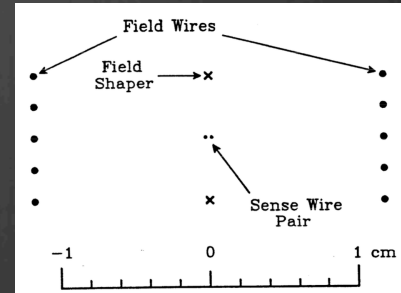
6:1
ARGUS
DORIS
1982

A square-shape, closed cell implies more uniform and t-to-d relations less dependent from the track angle

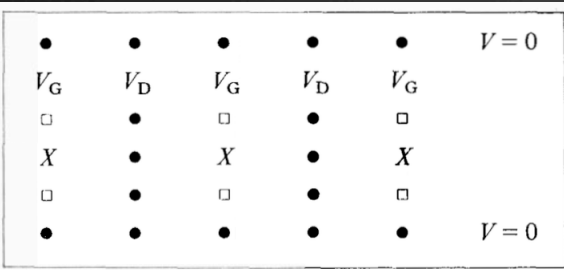
A larger ratio of field to sense wires allows for thinner field wires and, therefore, for less multiple scattering contribution from the wires to the momentum measurement.



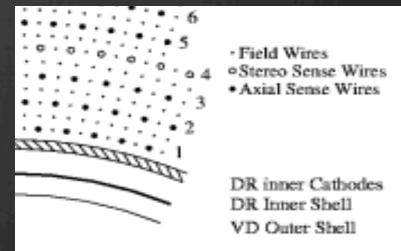
2:1
AMY
TRISTAN
1984



5:1
MAC
PEP
1980



5(7):1
DM2
DCI
1982



3:1
CLEO2
CESR
1985

Single sense wire "closed" cells

Mechanics

	MAC PEP (1980)	ARGUS DORIS (1982)	DM2 DCI (1982)	AMY TRISTAN (1984)	CLEO2 CESR (1984)
Inner Radius [mm]	120	150	325	148	175
Outer Radius [mm]	455	860	871	655	945
Length [mm]	1890	2000	2400	1800	1890
Axial layers	4	18	5	25	40
Stereo layers	6	18	8	15	11
Stereo angles [mrad]	± 50	$\pm 40 \div 80$	± 52	± 79	± 52
Number of sense wires	883	5940	2080	9048	12240
Total number of wires	6,500	31,000	17,000	32,000	49,000
sense wires [μm]	20 W(Au)	20 W-Re(Au)	20 W-Re(Au)	20 W(Au)	20 W(Au)
field wires [μm]	200 Cu-Be	120-200 Al(Au)	120-200 Al(Au)	160 Al(Au)	110 Al/Cu-Be(Au)
Inner cylinder [mm/ X_0]	? / 1.6%	3.3 C-f / 1.5%			0.75 C-f+1 Al / 1.5%
Outer cylinder [mm/ X_0]		6 Al / 6.7%			6.35 HC+1.6 Al / 3%
End-plates [mm/ X_0]	19 SS / 110%	30 Al / 34%			31.7 Al / 36%

Single sense wire "closed" cells Performance

	MAC PEP (1980)	ARGUS DORIS (1982)	DM2 DCI (1982)	AMY TRISTAN (1984)	CLEO2 CESR (1984)
B-field [T]	0.57	0.8	0.5	3.0	1.5
Cell Size [mm²]	(15÷23.5)×10	18×18.8	24×40	10×12	14×14
Gas Mixture	90 Ar / 10 CH ₄	97 C ₃ H ₆ / 3 C ₃ H ₆ O ₂	50 Ar / 50 C ₂ H ₆	50 Ne / 50 C ₂ H ₆	50 Ar / 50 C ₂ H ₆
Spatial Resolution [μm]	180	150	180	200	180
Momentum Resolution	0.052p / ?	0.009p / 0.010	0.014p / 0.014	0.0070p / ?	0.0026p / 0.0057
Δp [MeV/c] at 1 GeV/c	>52	13.5	19.8	>10	6.3
dE/dx	//	5.0%	TOF + Cer.	//	6.0%

Lesson #1 - from "open" to "closed" cell

- closed cells limit the very long tails in the drift time distribution
- closed cells make the time-to-distance relations less dependent from the track angle
- square cells make the time-to-distance relations more isotropic
- small drift distance limits drift asymmetries due to Lorenz angle

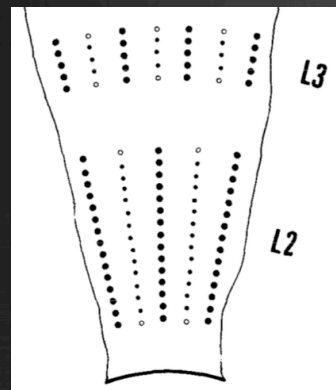
... but

- portions of active volume not sampled between the cylindrical envelope of axial wires and the hyperboloid envelope of stereo wires
- small ratio of the number of field wires per sense wire (3:1) forces the use of thick field wires with consequences on multiple scattering contribution to momentum resolution and total load on end-plates
- some problems with left-right ambiguity and close tracks separation

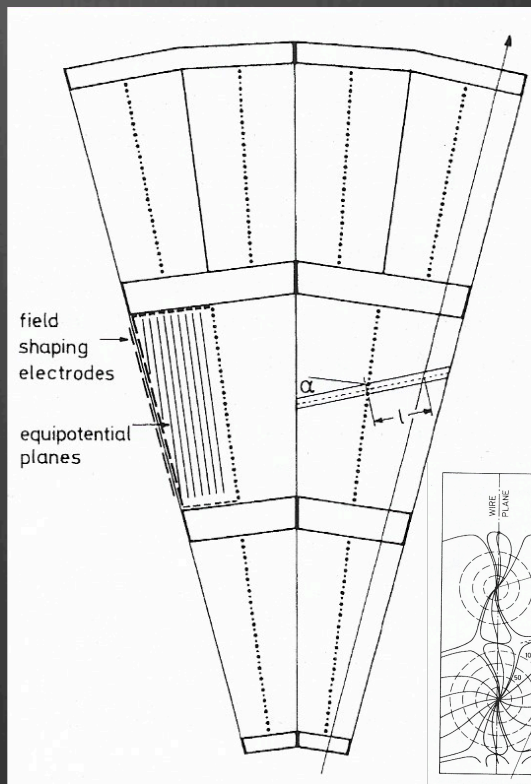
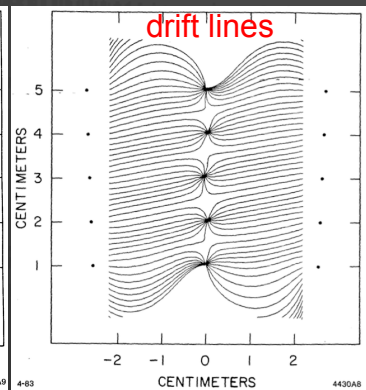
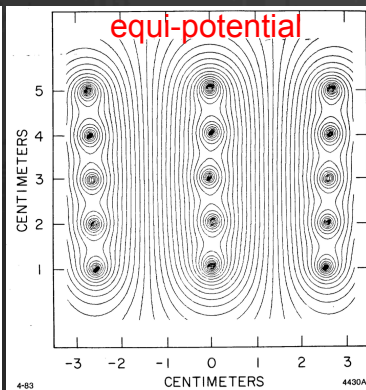
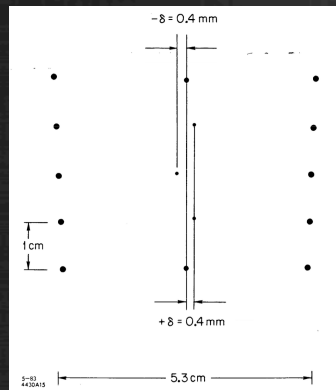
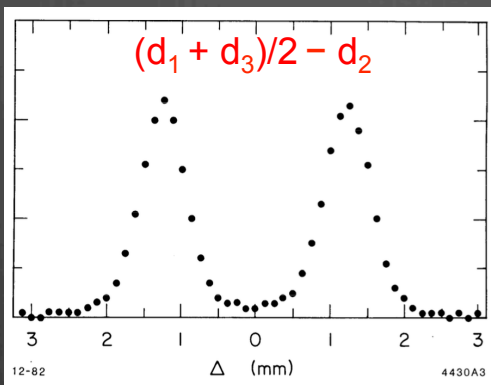
MARK3 at SPEAR – JADE at PETRA

F. Grancagnolo and A. Seiden, Large Drift Chambers with a Multi-Wire Cell Design, SCIPP 81/5

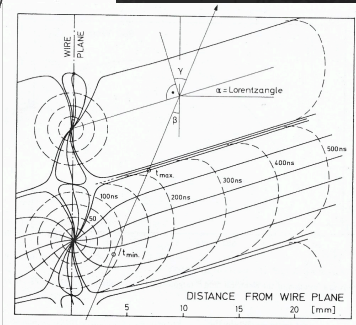
J. Heintze, Drift chambers and recent developments, NIM 156 (1978) 227



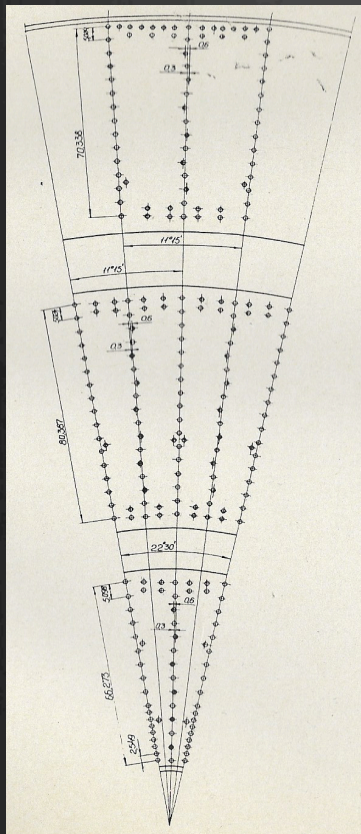
2.33:1
MARK3
SPEAR
1980



≈1:1
JADE
PETRA
1981

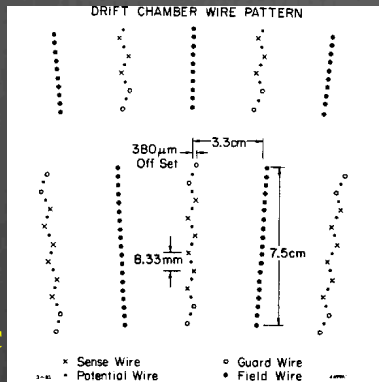


Multi-wire and Jet-like cells

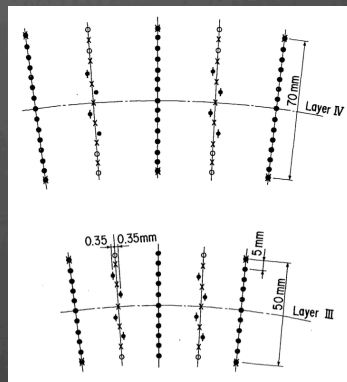


6.8:1
CMD-2
VEPP-2M
1985

5.3:1
MARK2
PEP/SLC
1985

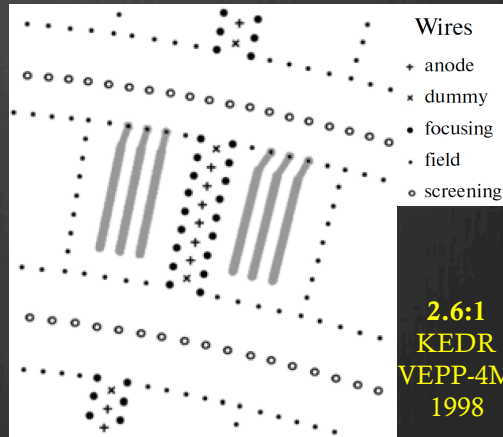
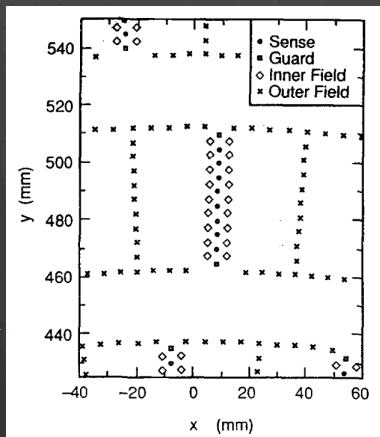
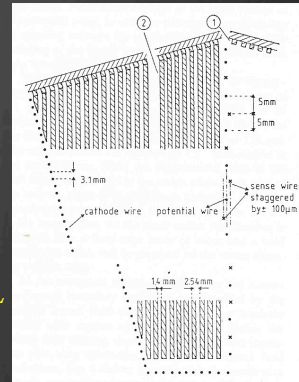


5.625:1
SLD
SLC
1988



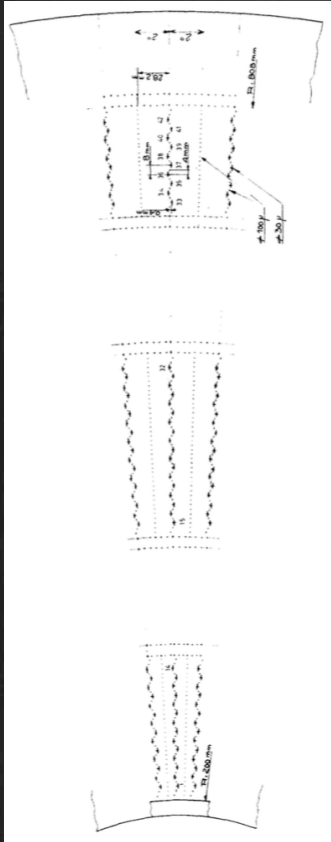
6.5:1
BES
BEPC
1989

4.3:1
OPAL
LEP
1988



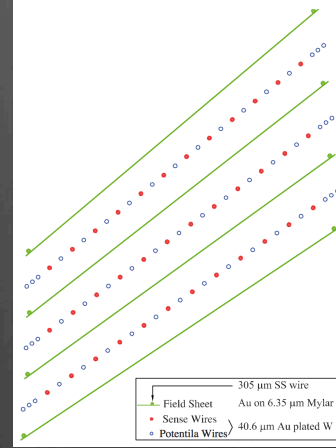
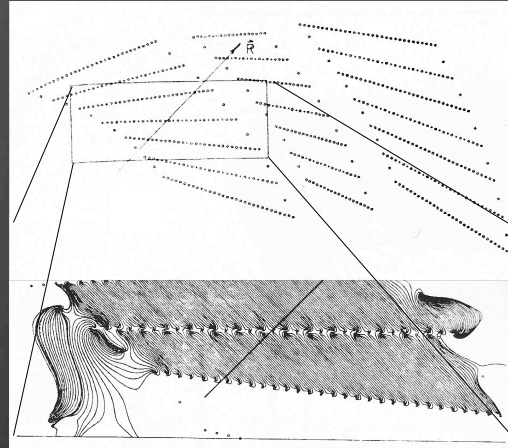
2.6:1
KEDR
VEPP-4M
1998

More Jet-like cells



5.625:1
AFS
ISR
1982

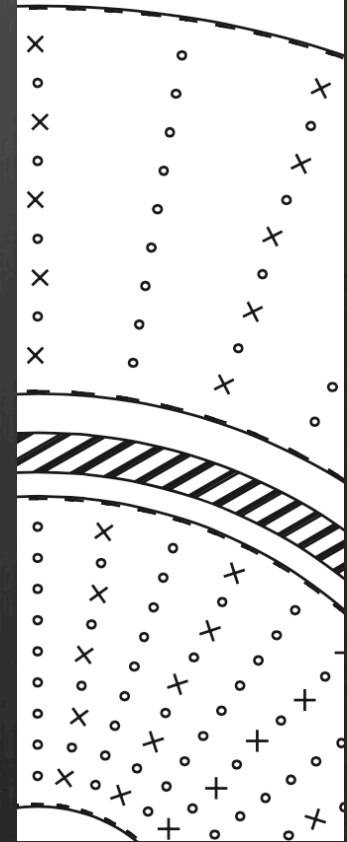
4.9:1
CDF CTC
Tevatron
1988



CDF COT
Tevatron
2002



4.25:1
ZEUS
HERA
1992



2.6:1
SND
VEPP-2M
1995

Multi-wire and Jet-like cells

Mechanics

	MARK3 SPEAR (1980)	JADE PETRA (1980)	CMD-2 VEPP-2M (1985)	MARK2 PEP/SLC (1985)	SLD SLC (1988)	OPAL LEP (1988)	BES/BESII BEPC (1989)	KEDR VEPP-4M (1998)
Inner Radius [mm]	140	180	25	192	200	245	155	125
Outer Radius [mm]	1140	800	295	1519	1000	1850	1150	535
Length [mm]	2337	2400	440	2300	2000	4000	2200	1100
Axial layers	12+4×3	16×2	6+7+6	6×6	4×8	159×1	5×4	4×6
Stereo layers	2×3	0	0	6×6	6×8	0	5×4	3×6
Stereo angles [mrad]	±150	0	0	±66	±41	0		±52
Number of sense wires	2000	1536	512	5832	5300	3816	2808	1512
Total number of wires	6,240	3360	3,500	37,000	35,000	20,000	19,400	16,000
sense wires [μm]	20 W(Au)/57 SS	25 W-Re(Au)	25 Ni-Cr	30 W(Au)	25 W(Au)	25 W-Re	30 W	28 W(Au)
field wires [μm]	175 Cu-Be	125-175 Cu-Be	10-20 Ti(Cu)	178-305 Cu-Be(Au)	150 Al(Au)	125-175 Cu-Be	100-178-200 Cu-Be	70-150 Ti(Au)
Inner cylinder [mm/X ₀]	9.5 HC+mylar+Al / 0.2%			2.0 Be / 0.6%	Al + HC	1.5 C-f / 0.7%		1.5 C-f / 0.7%
Outer cylinder [mm/X ₀]	6.25 Al / 7.0%			12.7 Al / 15.0%	Al + HC			5.0 G10 / 3.0%
End-plates [mm/X ₀]	25.4 / 15% - 7.62 / 8.5%	25.4 G10 / 15.0%	10.0 G10 / 6.0%	51.0 Al / 57.0%	5.0 Al / 5.7%	32 G10 / 19.2% / 28 Al / 33.0%		20 G10 / 12.0%

Multi-wire and Jet-like cells

Performance

	MARK3 SPEAR (1980)	JADE PETRA (1980)	CMD-2 VEPP2M (1985)	MARK2 PEP/SLC (1985)	SLD SLC (1988)	OPAL LEP (1988)	BES/BESII BEPC (1989)	KEDR VEPP4M 1998)
B-field [T]	0.4	0.45	2.0	0.4	0.6	0.44	0.4	0.6 (1.8)
Cell Size [mm²]	(18+30)×10	(10+30)×10	(16+28)×10	33×8.33	60×50	(30+250)×10	30×10	30×4.5
Gas Mixture	HRS gas	88.7 Ar / 8.5 CH ₄ / 2.8 iC ₄ H ₁₀	80 Ar / 20 iC ₄ H ₁₀	HRS gas	21 Ar / 72 CO ₂ / 4 iC ₄ H ₁₀	88 Ar / 10 CH ₄ / 2 iC ₄ H ₁₀ at 4 bar	HRS gas	C ₂ H ₂ O (DME)
Spatial Resolution [μm]	220	135-165	95	175	155	135	240	115
Momentum Resolution	0.015p / 0.015	0.022p / ?	? / ?	0.0015p / 0.014	0.010p / 0.005	0.00150p / 0.02	0.018p / 0.018	0.02p / 0.03
Δp [MeV/c] at 1 GeV/c	21	>22	50	14.1	11.1	20	25	36
dE/dx	15.0%	6.0% - 8.5%	//	7.0%	6.4%	3.1% - 3.8%	8.5%	8.5%

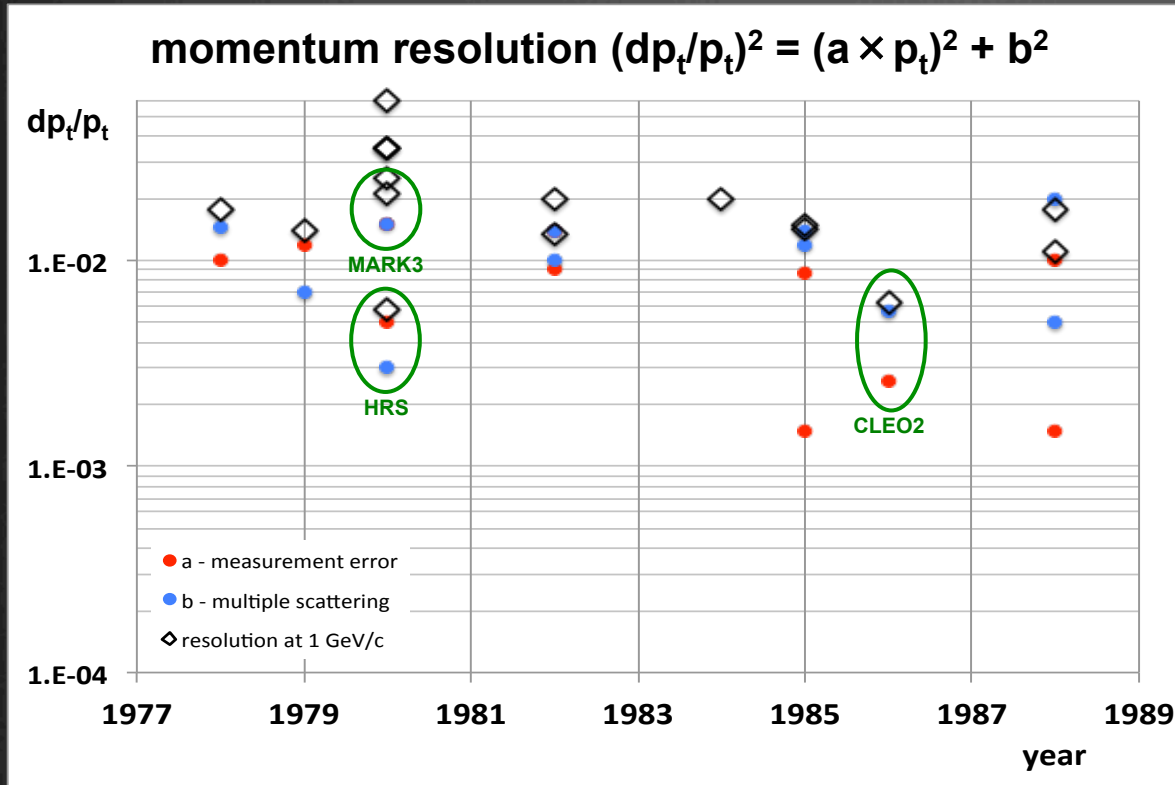
Lesson #2 - from single to multi-wire

- left-right ambiguity solved at the cell level
- track finding facilitated by the definition of a point and a vector within a single cell
- double track resolution improved with suitable front-end electronics

... but

- very long drift times
- portions of active volume not sampled between the cylindrical envelope of axial wires and the hyperboloid envelope of stereo wires
- need for extra (thick) wires to limit cross-talk between adjacent sense wires and for extra wires at cell boundary to limit long drifts
- only limited stereo angles allowed because of its radial dependence for long jet-like cells

Momentum resolution in early chambers



$$(dp_t/p_t)^2 = [8\sqrt{5}\sigma_{r\phi}/(0.3BL^2\sqrt{N})]^2 p_t^2 + [5.4 \times 10^{-2}/BL\sqrt{(L/X_0)}]^2$$

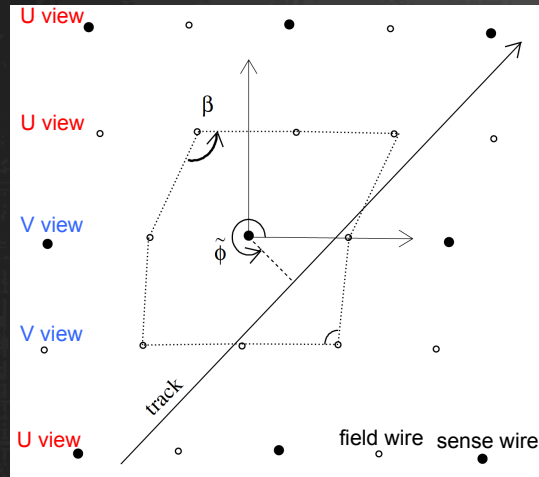
Despite the large variety of different parameters involved, **momentum resolution** (at $p=1\text{GeV}/c$) clusters around **1-2%** for all chambers.

Initially, resolution dominated by the **sagitta measurement error**. With improved cell configurations, the dominant error became **multiple scattering**, claiming for a **breakthrough** in the **gas mixture** and in the **wires**.

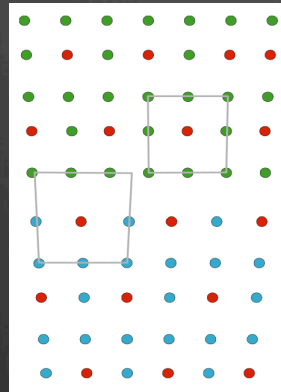
Helium as Drift Chamber gas ...

- W. Zimmermann et al., *Helium-propane as drift chamber gas*, Nucl. Instrum. Meth. A243 (1986) 86
- F. Grancagnolo, *A Helium Drift Chamber as the Central Tracker of a B-Factor*, Proc. Workshop on Heavy Quarks Factory and Nuclear Physics Facility with Superconducting Linacs, Courmayeur, 1987, eds. E. De Sanctis, M. Greco, M. Piccolo and S. Tazzari (Atti di Conferenze, Società Italiana di Fisica, Bologna 1987) p. 599
- F. Grancagnolo, *A Central Tracking Detector for a B-Factor*, Nucl. Instrum. Meth. A277 (1989) 110

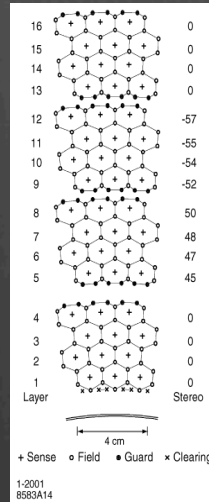
... and back to single sense wire cells



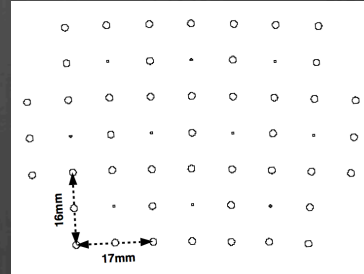
KLOE



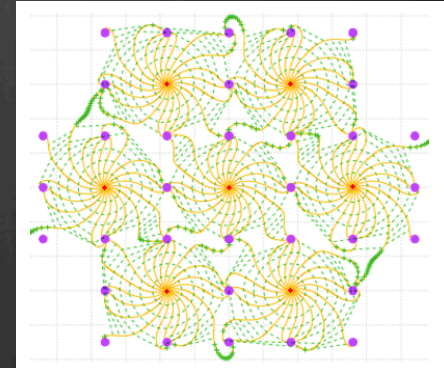
CLEO3



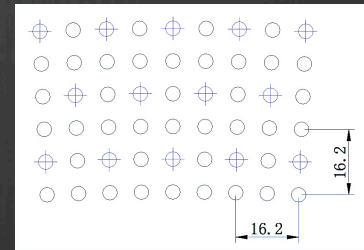
BABAR



BELLE



BELLE2



BES3

Single wire cells – He gas Mechanics

	BESIII BEPC2 (2008)	KLOE DAPHNE (1998)	CLEO3 CESR2 (1998)	BABAR PEP2 (1998)	BELLE KEKB (1998)	BELLE2 KEKB (2017)
Inner Radius [mm]	63	250	125	236	77	160
Outer Radius [mm]	810	1980	820	808	880	1130
Length [mm]	2400	3300	2500	2800	2400	2420
Axial layers	5×4	0	8×2	4×4	6×5	5×6
Stereo layers	6×4	12+46	8×4	6×4	5×4	4×6
Stereo angles [mrad]	±35÷50	±60÷150	±20÷30		±42÷74	±60÷80
Number of sense wires	7000	12582	9796	7104	8400	14,336
Total number of wires	29,000	52,000	40,000	25,000	35,000	60,000
sense wires [μm]	25 W-Re(Au)	25 W(Au)	20 W-Re(Au)	20 W-Re(Au)	30W(Au)	30 W(Au)
field wires [μm]	110 Al(Au)	80 Al(Ag)	110 Al(Au)	80-120 Al(Au)	126 Al	126 Al
Inner cylinder [mm/X ₀]	1.0 C-f / 0.45%	0.75 C-f + 0.2 Al / 0.55%	2.0 Roh + Al / 0.12%	1.0 Be / 0.28%	2.0 C-f / 1.1%	0.4 C-f / 0.22%
Outer cylinder [mm/X ₀]	11.0 C-f / 5.0%	3.0 C-f + HC / 2.5%		C-f + HC / 1.5%	5.0 C-f / 2.6%	5.0 C-f / 2.6%
End-plates [mm/X ₀]	25.0 Al / 28.0%	9.0 C-f / 4.7%	15.5 Al + ... / 17%	12/24 Al / 13.5%/27.0%	10.0 Al / 11.0%	10.0 Al / 11.0%

Single wire cells – He gas Performance

	BESIII BEPC2 (2008)	KLOE DAPHNE (1998)	CLEO3 CESR2 (1998)	BABAR PEP2 (1998)	BELLE KEKB (1998)	BELLE2 KEKB (2017)
B-field [T]	1.0	0.6	1.5	1.5	1.5	1.5
Cell Size [mm²]	12×12 ÷ 16×16	20×21 + 30×31.5	14×14	12×18	8×15.5 + 10×17	87.5 + 15,25
Gas Mixture	60 He / 40 C ₂ H ₆	90 He / 10 iC ₄ H ₁₀	60 He / 40 C ₂ H ₆	80 He / 20 iC ₄ H ₁₀	50 He / 50 C ₂ H ₆	50 He / 50 C ₂ H ₆
Spatial Resolution [μm]	120	200	110	125	130	130
Momentum Resolution	0.0032p / 0.0037	0.0005 / 0.0026	0.0016p / 0.0028	0.0015p / 0.0045	0.0019p / 0.0030	0.0011p / 0.0025
Δp [MeV/c] at 1 GeV/c	4.9	2.6	3.2	4.7	3.5	2.7
dE/dx	6%-7%	4.6%	5.0%	7.5%	6.9%	6.9%

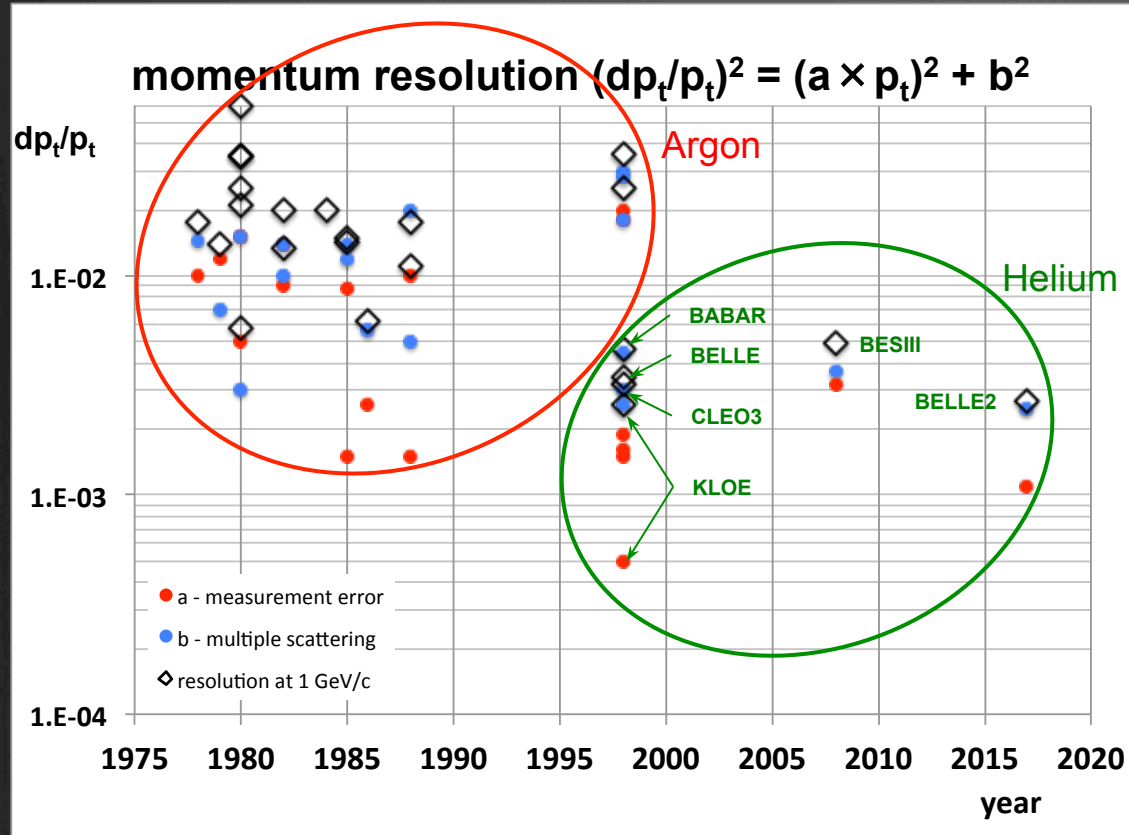
Lesson #3 – small cells and He gas

- He radiation length $50\times$ longer than Ar
- slower drift velocity implies smaller Lorenz angle for a given B-field
- He has a smaller cross section for low energy photons than Ar
- small size cells limit the electron diffusion contribution to spatial resolution
- small size cells provide high granularity (improving occupancy) and allow for a larger number of hits per track, improving spatial resolution

... but

- portions of active volume not sampled between the cylindrical envelope of axial wires and the hyperboloid envelope of stereo wires
- accumulation of trapped electrons and ions in a region of very low field
- longitudinal gain variation at boundaries between axial and stereo layers
- spatial resolution dominated by ionization statistics for short drift distances
- adding more quencher to compensate, mitigates the advantage of He

Momentum resolution after Helium



$$(dp_t/p_t)^2 = [8\sqrt{5}\sigma_{r\phi}/(0.3BL^2\sqrt{N})]^2 p_t^2 + [5.4 \times 10^{-2}/BL\sqrt{(L/X_0)}]^2$$

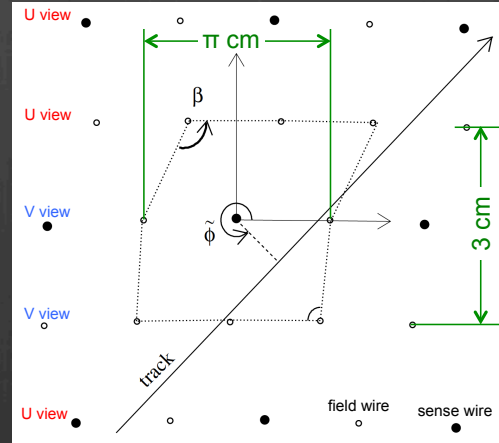
Momentum resolution
 \leq a few $\times 10^{-3}$

However,
too large amounts of
quencher mitigate
the advantages of the
long radiation length
of Helium

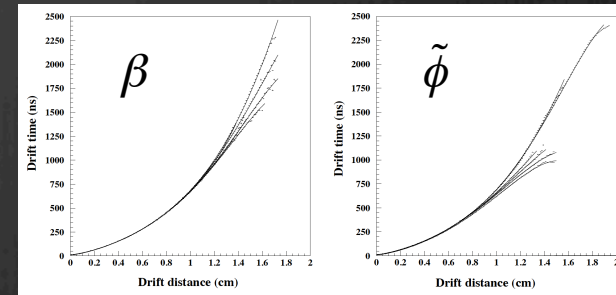
"Full" stereo configuration: KLOE

A configuration with only perfectly nested alternating sign stereo layers (no axial layer) fills the gaps occurring in a mixed stereo-axial configuration, rendering the the chamber more isotropic and fully sampled, thus increasing the number of hits on a track for a given cell size.

In **KLOE**, this is achieved by having the field wires layer of the cell outer bound at a stereo angle of opposite sign w.r.t. the sense wire layer and to the field wires layer of the cell inner bound



The stereo configuration is obtained with constant stereo drop at the middle transverse plane. This, however, besides causing a small longitudinal variation of the cell aspect ratio, implies: **time to distance relations which depend on the track angle and on the cell periodicity in z.**



Lesson #4 – full stereo configuration

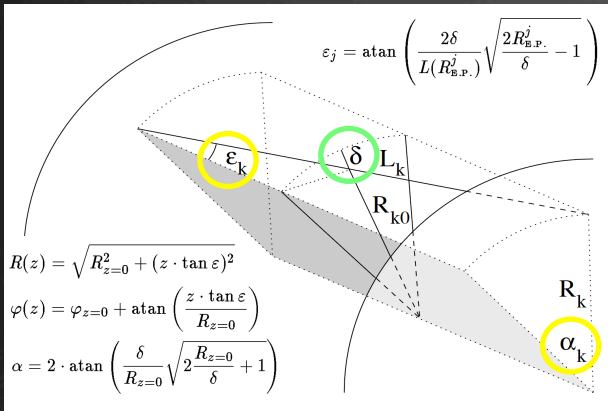
- no gaps between axial and stereo layers which may trap ions and electrons in regions of very low electric field
- constant sense wire gain as a function of the longitudinal coordinate
- larger number of hits on a track for a given cell size
- maximizes the number of measurements of the longitudinal coordinate
- two stereo views enable 3D reconstruction in a natural way

... but

- open top cells cause a dependence of the time-to-distance relations from the track angle and from the cell longitudinal periodicity
- constant stereo drop (as in KLOE) changes the cell aspect ratio along z (radial cell size constant but azimuthal width increased at end-plates)
- constant stereo angle generates cell distortions for large stereo angles

MEG2 approach at "full" stereo

see Tassielli, next talk

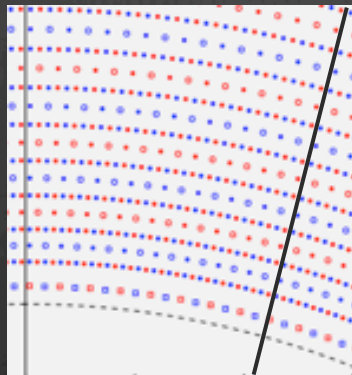
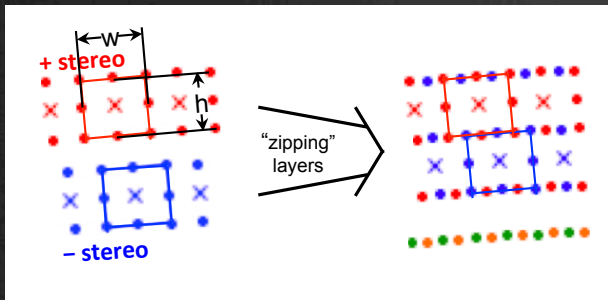


Constant **transverse stereo angle projection** α_k preserves the cell aspect ratio:

"square" cells by construction: $w_k = h_k$ remain such **at any z**
 $[w_k(z=\pm L/2) = h_k(z=\pm L/2) = 1.035 w_k(z=0) = 1.035 h_k(z=0)$
 for 100 mrad stereo angle and 2 m wire length]

no β angle dependence - no Φ angle dependence
 in principle, **one single t-to-d scalable for all layers**

Layer assembly

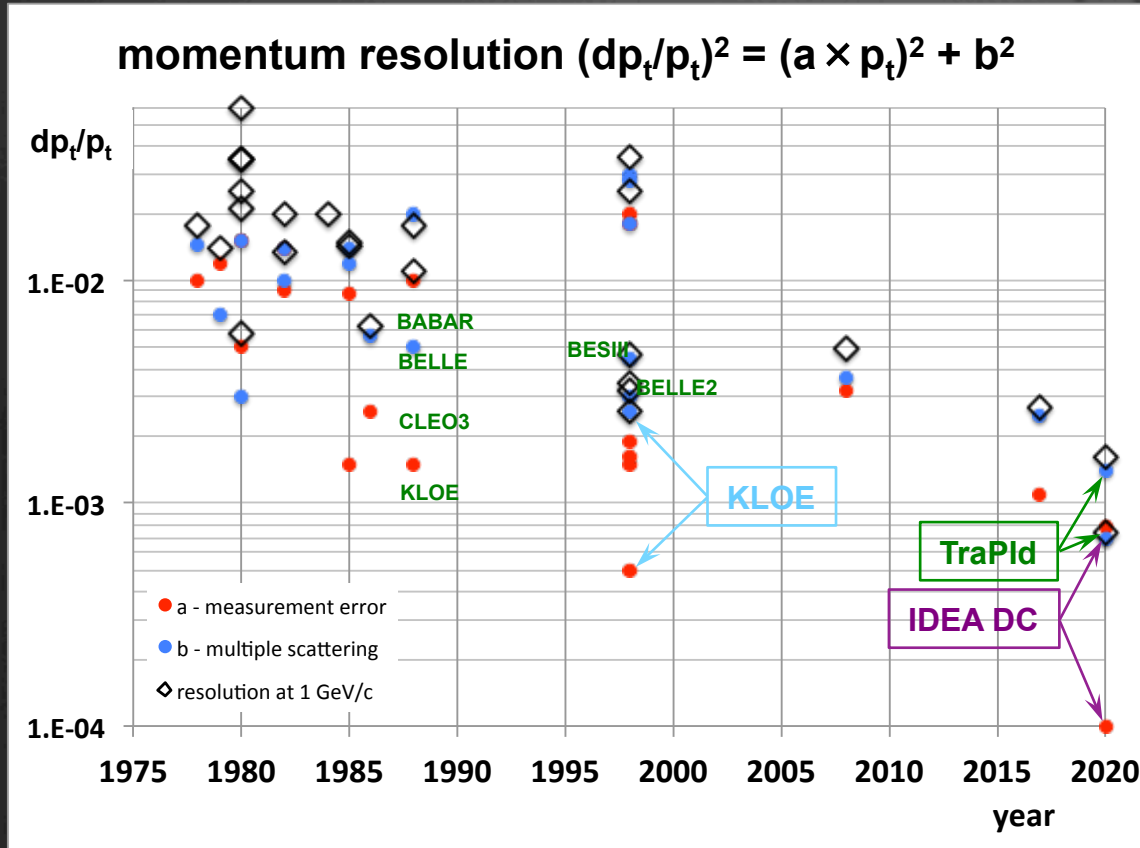


This configuration requires more **field wires per sense wire**
(5:1, as opposed to 3:1 in KLOE)
 allowing for **thinner field wires**,
 therefore, even **less m.s. contribution**
 and **less load on the end plates.**

Lesson #5 – summary

- the configuration offering the best performance in terms of **momentum resolution** is one with **small, single** sense wire **closed cells**, arranged in **contiguous layers of opposite sign stereo angles**, obtained with **constant stereo angle transverse projection**
- the gas mixture is based on helium with a small amount of quencher (**90% He / 10% iC_4H_{10}** , **KLOE gas**) which, besides low multiple scattering contribution, allows for the exploitation of the **cluster timing** technique, for improved spatial resolution, and of the **cluster counting** technique, for excellent particle identification
- suggested wire material is **Ag coated Al**, but lighter materials are under scrutiny (like **metal coated carbon monofilaments**)

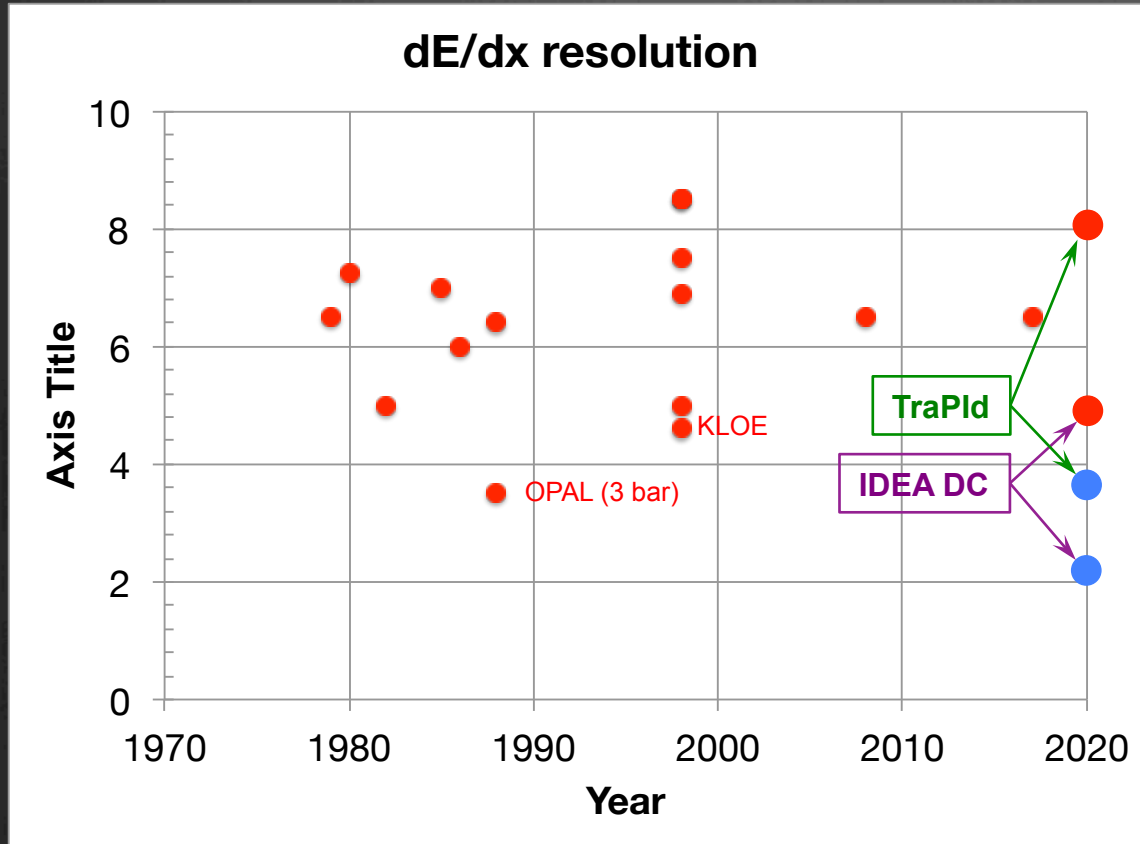
IDEA DC and TraPId p_t resolution



IDEA DC
proposed for the IDEA
detector
at FCC-ee and CEPC

TraPId
TRACKing and
Particle Identification
Drift Chamber for
SCTF at BINP

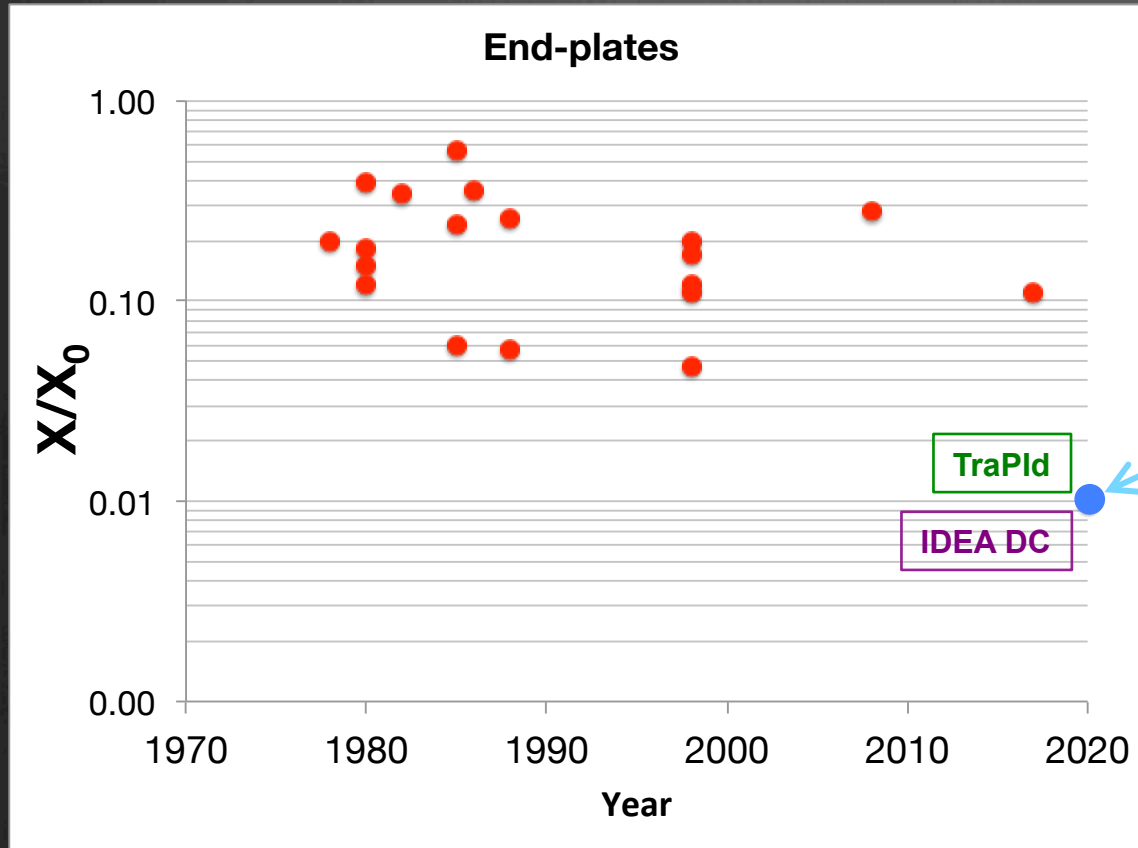
IDEA DC and TraPId dE/dx resolution



● dE/dx

● dN/dx

IDEA and TraPId end-plate X_0



please,
have a look at **Poster #91**
"New Concepts for Light
Mechanical Structures of
Cylindrical Drift Chambers"

Conclusions

- we have presented the evolution of **momentum resolution** for drift chambers at e^+e^- colliders over the past 40 years
- we have briefly summarized the **particle identification** capabilities with **dE/dx** and the potentialities with cluster counting (**dN/dx**)
- we have briefly listed the impact of the drift chambers **mechanical structure** as passive material in front of the electromagnetic end-caps calorimeters and the relative improvements over the years
- we have **not** discussed about the **front-end electronics** evolution and the different techniques of **data acquisition** and **processing** of the wire signals.

Momentum and Angular Resolutions

<https://doi.org/10.1016/j.nima.2018.08.078>

An extension of the Gluckstern formulae for multiple scattering: Analytic expressions for track parameter resolution using optimum weights



Z. Drasal^{a,b}, W. Riegler^{b,*}

^a Charles University, Prague, Czech Republic
^b CERN EP, Geneva, Switzerland

ARTICLE INFO

ABSTRACT

Keywords:

Tracking
Multiple scattering
Impact parameter resolution
Momentum resolution

Momentum, track angle and impact parameter resolution are key performance parameters that tracking detectors are optimised for. This report presents analytic expressions for the resolution of these parameters for equal and equidistant tracking layers. The expressions for the contribution from position resolution are based on the Gluckstern formulae and are well established. The expressions for the contribution from multiple scattering using optimum weights are discussed in detail.

$$\begin{aligned} \frac{\Delta p_T}{p_T} \Big|_{res.} &= \frac{\sigma_{r\phi} p_T}{0.3 B_0 L_0^2} \sqrt{\frac{720 N^3}{(N-1)(N+1)(N+2)(N+3)}} \\ &\approx \frac{12 \sigma_{r\phi} p_T}{0.3 B_0 L_0^2} \sqrt{\frac{5}{N+5}} \\ \frac{\Delta p_T}{p_T} \Big|_{m.s.} &= \frac{N}{\sqrt{(N+1)(N-1)}} \frac{0.0136 \text{ GeV}/c}{0.3 \beta B_0 L_0} \\ &\times \sqrt{\frac{d_{tot}}{X_0 \sin \theta}} \left(1 + 0.038 \ln \frac{d}{X_0 \sin \theta} \right) \\ &\approx \frac{0.0136 \text{ GeV}/c}{0.3 \beta B_0 L_0} \sqrt{\frac{d_{tot}}{X_0 \sin \theta}} \end{aligned}$$

$$\begin{aligned} \Delta d_0|_{res.} &= \frac{3\sigma_{r\phi}}{\sqrt{(N-1)(N+1)(N+2)(N+3)}} \times \\ &\sqrt{\left(N^3 - \frac{N}{3} - \frac{2}{3} \right) + \frac{4(2N^3 - N^2 - N)r_0}{L_0} + \frac{4(7N^3 - N^2 - N)r_0^2}{L_0^2} + \frac{40N^2 r_0^3}{L_0^3} + \frac{20N^2 r_0^4}{L_0^4}} \\ &\approx \frac{3\sigma_{r\phi}}{\sqrt{N+3}} \sqrt{1 + \frac{8r_0}{L_0} + \frac{28r_0^2}{L_0^2} + \frac{40r_0^3}{L_0^3} + \frac{20r_0^4}{L_0^4}} \\ \Delta d_0|_{m.s.} &= \frac{r_0}{\beta p_T} f \left(\frac{d}{X_0 \sin \theta} \right) \sqrt{\frac{N-3/4}{N-1} + \frac{N}{2(N-1)} \left(\frac{r_0}{L_0} \right) + \frac{N^2}{4(N-1)} \left(\frac{r_0}{L_0} \right)^2} \\ \Delta d_0|_{m.s.}^{opt} &= \frac{r_0}{\beta p_T} f \left(\frac{d}{X_0 \sin \theta} \right) \sqrt{1 + \left(\frac{r_0}{L_0} \right) + \left(\frac{r_0}{L_0} \right)^2} \quad N_{opt} = 2 + \frac{L_0}{r_0} \\ &\approx \frac{0.0136 \text{ GeV}/c}{\beta p_T} \frac{r_0}{X_0 \sin \theta} \sqrt{1 + \left(\frac{r_0}{L_0} \right) + \left(\frac{r_0}{L_0} \right)^2} \end{aligned}$$

$$\begin{aligned} \Delta z_0|_{res.} &= \frac{2\sigma_z}{\sqrt{(N+1)(N+2)}} \sqrt{\left(N + \frac{1}{2} \right) + \frac{3Nr_0}{L_0} + \frac{3Nr_0^2}{L_0^2}} \\ &\approx \frac{2\sigma_z}{\sqrt{N+3}} \sqrt{1 + \frac{3r_0}{L_0} + \frac{3r_0^2}{L_0^2}} \\ \Delta z_0|_{m.s.} &= \frac{r_0}{\sin \theta \beta p_T} f \left(\frac{d}{X_0 \sin \theta} \right) \\ &\approx \frac{0.0136 \text{ GeV}/c}{\beta p_T} \frac{r_0}{\sin \theta} \sqrt{\frac{d}{X_0 \sin \theta}} \end{aligned}$$

$$\begin{aligned} \Delta \theta|_{res.} &= \frac{\sigma_z \sin^2 \theta}{L_0} \sqrt{\frac{12N}{(N+1)(N+2)}} \\ &\approx \frac{2\sigma_z \sin^2 \theta}{L_0} \sqrt{\frac{3}{N+3}} \\ \Delta \theta|_{m.s.} &= \frac{\sin \theta}{\beta p_T} f \left(\frac{d}{X_0 \sin \theta} \right) \\ &\approx \frac{0.0136 \text{ GeV}/c \sin \theta}{\beta p_T} \sqrt{\frac{d}{X_0 \sin \theta}} \end{aligned}$$

$$\begin{aligned} \Delta \phi|_{res.} &= \frac{\sqrt{12} \sigma_{r\phi}}{L_0 \sqrt{(N-1)(N+1)(N+2)(N+3)}} \\ &\times \sqrt{\left(16N^3 + 2N^2 - 3N \right) + \frac{60N^3 r_0}{L_0} + \frac{60N^3 r_0^2}{L_0^2}} \\ &\approx \frac{\sigma_{r\phi}}{L_0} \frac{8\sqrt{3}}{\sqrt{N+5}} \sqrt{1 + \frac{15 r_0}{4 L_0} + \frac{15 r_0^2}{4 L_0^2}} \\ \Delta \phi|_{m.s.} &= \frac{1}{\beta p_T} f \left(\frac{d}{X_0 \sin \theta} \right) \\ &\times \sqrt{\frac{N-3/4}{N-1} + \frac{N}{N-1} \left(\frac{r_0}{L_0} \right) + \frac{N^2}{N-1} \left(\frac{r_0}{L_0} \right)^2} \\ \Delta \phi|_{m.s.}^{opt} &= \frac{1}{\beta p_T} f \left(\frac{d}{X_0 \sin \theta} \right) \\ &\times \sqrt{1 + 2 \left(\frac{r_0}{L_0} \right) + 4 \left(\frac{r_0}{L_0} \right)^2} \quad N_{opt} = 2 + \frac{1}{2} \frac{L_0}{r_0} \\ &\approx \frac{0.0136 \text{ GeV}/c}{\beta p_T} \sqrt{\frac{d}{X_0 \sin \theta}} \sqrt{1 + 2 \left(\frac{r_0}{L_0} \right) + 4 \left(\frac{r_0}{L_0} \right)^2} \end{aligned}$$

dE/dx and dN_{cl}/dx Resolutions

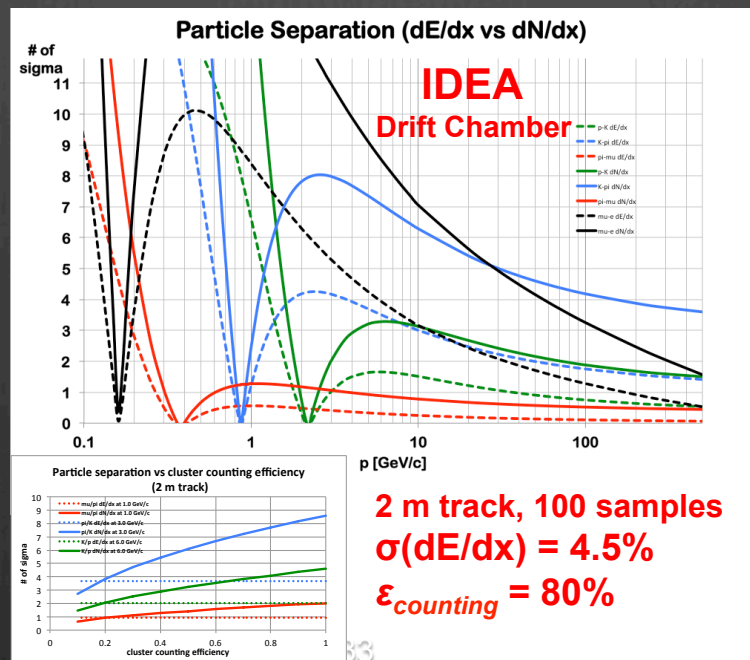
$$\frac{\sigma_{dE/dx}}{(dE/dx)} = 0.41 \cdot n^{-0.43} \cdot (L_{track} [m] \cdot P[atm])^{-0.32}$$

A. H. Walenta et al., *Measurement of the ionization loss in the region of relativistic rise for noble and molecular gases*, Nucl. Instr. and Meth. 161 (1979) 45-58.

$$\frac{\sigma_{dN_{cl}/dx}}{(dN_{cl}/dx)} = (\epsilon_{counting} \cdot \delta_{cluster} \cdot L_{track})^{-0.5}$$

G. Cataldi, F. Grancagnolo and S. Spagnolo, *Cluster counting in helium based gas mixtures*, Nucl. Instr. and Meth. A386 (1997) 458-469.

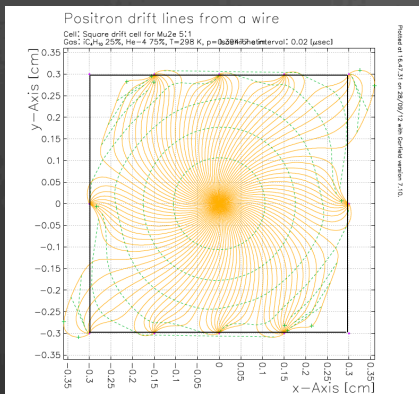
- ❖ 5-80% truncated mean method
- ❖ statistical fluctuations of gas gain (< 1%)
 - drift distance dependence
 - z-dependence along the wire
 - wire sagging ($\Delta w/w < 3 \times 10^{-3}$)
- ❖ statistical fluctuation of energy loss (Landau)
- ❖ attachment (gas quality)
- ❖ avalanche saturation (angle dependence)
- ❖ rate effects
- ❖ double track separation
- ❖ wire to wire calibration



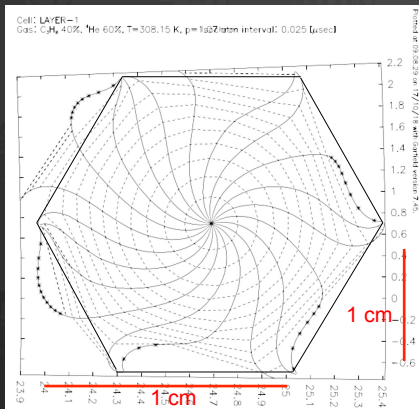
- ❖ Poisson statistics
- ❖ $\delta_{cluster} = 12.5$ cluster/cm in (90%He-10%iC₄H₁₀)
- ❖ outperforms dE/dx by a factor $\times 2$
- ❖ even at very low counting efficiency ($\epsilon_{counting} \approx 20\%$) better than dE/dx
- ❖ insensitive to
 - gas gain variations
 - lower dependence on gas composition
 - slighter dependence on avalanche saturation
- ❖ no wire to wire calibration needed

Square versus Hexagonal cells

$B = 1\text{ T}$
75%He-25% $i\text{C}_4\text{H}_{10}$

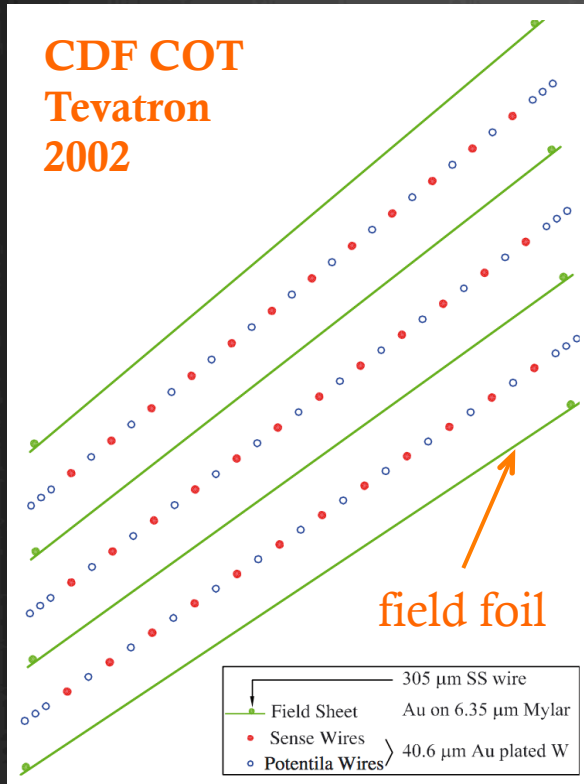




$B = 1.5\text{ T}$
60%He-40% C_3H_8



- small deviation of equi-time from perfect polygonal shape: 3.3% vs. 3.1%
- field to sense wire ratio: 5 to 1 vs. 2 to 1 for equal gain
 - more field wires implies more isotropic E-field and smaller distortions due to the $E \times B$ effects
 - thinner field wires: 40 μm vs. 100-125 μm
 - less multiple scattering
 - less load on end plates
- smaller gaps in B-field
- larger time-to-distance distortions
 - longer tails (> 500 ns for 1 cm cell) in signal pulse (hit pattern, dE/dx , pile up)
- easier implementation of a full stereo configuration

field foil versus field wires



- very effective solution to confine broken wires within a limited region
- very uniform field at the cell boundary
- larger cathode surface allows for running at higher gain
- no such a radial symmetry with single sense wire cells
- azimuthal symmetry for axial wire layers but not for stereo layers
- Moreover:
 - 6.35 μm Mylar + 2×0.035 μm Au  = $2.4 \times 10^{-4} X_0$
 - 40 μm diameter Au plated Al (4/cm)  = $1.0 \times 10^{-5} X_0$
- Load on end plates: 560 g/cm of foil, 80 g for 4 wires/cm